Journal of the Serbian Chemical Society
JSCS-info@shd.org.rs • www.shd.org.rs/JSCS

# ACCEPTED MANUSCRIPT

Journal of the Serbian Chemical Society
JSCS-info@shd.org.rs • www.shd.org.rs/JSCS
*J. Serb. Chem. Soc.* **00(0)** 1-17 (2026)
*JSCS–13693*
*Original scientific paper*
Published DD MM, 2026



# The effect of catalyst composition and surface properties on the selective catalytic dehydrogenation of bioethanol

GUNEL R. AZIMOVA[1]*, SELIME MAMMADOVA[2], TURANA A. BABAYEVA[3], KONUL SH. ALAKBAROVA[1], VILAYET S. MAMMADOV[1], TIANJIN LI[4], AND ELMIR M. BABAYEV[1,3]**

*[1]Chemistry Institute, H.Javid Ave. 113, AZ1143, Baku, Azerbaijan, [2]Azerbaijan State Oil and Industry University, Azadlıq 20, AZ 1010, Baku, Azerbaijan, [3]Baku Engineering University, Hasan Aliyev st., 120, AZ0101, Khirdalan, Azerbaijan, and [4]Energy Research Institute, Qilu University of Technology, Shandong Academy of Sciences, Jinan 250014, PR China.*

(Received 27 December 2025; revised 21 January; accepted 11 May 2026)

*Abstract:* The article provides a comparative analysis of bioethanol dehydrogenation using Cr-Cu-O and Ce-Cu-O catalyst systems. For the Cr-Cu-O catalysts, bioethanol is converted into a range of products including acetaldehyde, acetone, ethylene. Advanced characterization revealed that these catalysts are structurally complex, containing not only just individual copper and chromium oxides but also a distinct compound, $Cu_2CrO_4$. A key finding is the clear structure-property relationship: the catalyst's crystallinity, which varied widely from 41.9% (mostly amorphous) to 73.8% (highly crystalline), has a major effect on its catalytic activity. The Ce-Cu-O system converted bioethanol into a diverse mixture of products such as acetaldehyde, acetone, and ethyl acetate, indicating the occurence of multiple simultaneous reactions, including dehydrogenation and condensation. Most compositions result in separate $CeO_2$ and CuO phases; however, a specific Ce:Cu ratio of 1:9 is unique. At this ratio, the material reduced to form $CeO_2$ with elemental copper, rather than CuO, and its crystallinity increases from 52.7% to 71.2%. The research shows that structural order is crucial for steering the reaction pathway, as only catalysts with low crystallinity produce ethyl acetate. Furthermore, while the specific surface area of a catalyst (5.0 to 17.0 $m^2/g$ in this study) is a key factor in surface-driven reactions such as dehydrogenation, it does not affect all products equally.

*Keywords:* acetaldehyde; binary Ce-Cu-O catalysts; binary Cr-Cu-O catalysts; specific surface area; X-ray diffraction.

## INTRODUCTION

Bioethanol[1-4] is produced from renewable biomass resources, including sugarcane, corn, lignocellulosic feedstocks, and even micro- and macroalgae.[5-6]

* Corresponding author. E-mail: ezimova2015@gmail.com; **elmir.magsadoglu@gmail.com
https://doi.org/10.2298/JSC251227024A

Beyond its widespread use as a biofuel, bioethanol serves as a versatile chemical platform molecule, acting as a pivotal precursor for the synthesis of numerous industrially important chemicals, fuels, and value-added materials.[7] Its renewable origin, coupled with its inherent chemical reactivity and compatibility with existing conversion technologies, makes bioethanol an essential building block in sustainable chemical manufacturing pathways and an important driver for the transition toward circular and low-carbon bio-based industries. Bioethanol can undergo multiple catalytic transformations, including dehydrogenation, dehydration, oxidation, esterification, amination etc.[8-10] Consequently, the design and development of advanced catalysts are a primary focus of ongoing research aimed at optimizing this transformative technology. The bioethanol dehydrogenation reaction is a typical example of a heterogeneous catalytic process. This means the reaction takes place not within a uniform solution, but on the surface of a solid catalyst.[11-13] The physical and chemical properties of this solid surface-such as its acidity, the arrangement of its atoms, and its pore structure-are critical in controlling the reaction's speed, selectivity (which products are formed), and overall efficiency.[14,15] The catalytic process is highly dependent on the physical makeup of the catalyst's surface. Its structural and textural characteristics, particularly the specific surface area ($m^2/g$), are vital as they dictate how many active sites are available for the reaction to occur. This availability is the primary factor controlling the catalyst's activity, selectivity, and operational efficiency. Essentially, a larger internal surface area gives the chemical reaction more room to occur, which improves performance.

Bioethanol dehydrogenation is a well-studied and industrially vital process, primarily for producing acetaldehyde-a key intermediate in synthesizing acetic acid, acetone, and other chemicals.[16] Through this reaction, other valuable products like ethyl acetate, acetone, and diethyl ether can also be obtained.

Copper-based catalysts are highly selective for this reaction, but their practical use is limited by stability issues.[24,25] To address this, modification with secondary metal oxides is common. In recent years, binary metal oxide systems, particularly chromium-copper (Cr–Cu–O) and cerium-copper (Ce–Cu–O) oxides, have gained significant attention for their enhanced catalytic activity, selectivity, and thermal stability. While copper oxide (CuO) alone is active, the incorporation of $Cr_2O_3$ or $CeO_2$ creates synergistic effects that improve catalyst stability, enhance redox properties, and favorably modify the surface structure. For instance, in Cr–Cu–O systems, a mixed copper chromite ($CuCr_2O_4$) phase can form, which is highly active. In Ce–Cu–O systems, the presence of $CeO_2$, CuO, and metallic Cu phases depends on the synthesis conditions, and these structural variations strongly influence catalytic behavior.[26,27] Copper-based catalysts are highly selective for this reaction, but their practical use is limited by stability issues. To address this, modification with secondary metal oxides is common. In recent years, binary metal

oxide systems, particularly chromium-copper (Cr–Cu–O) and cerium-copper (Ce–Cu–O) oxides, have gained significant attention for their enhanced catalytic activity, selectivity, and thermal stability.[17-19] While copper oxide (CuO) alone is active, the incorporation of $Cr_2O_3$ or $CeO_2$ creates synergistic effects that improve catalyst stability, enhance redox properties, and favorably modify the surface structure. For instance, in Cr–Cu–O systems, a mixed copper chromite ($CuCr_2O_4$) phase can form, which is highly active. In Ce–Cu–O systems, the presence of $CeO_2$, CuO, and metallic Cu phases depends on the synthesis conditions, and these structural variations strongly influence catalytic behavior.

A primary factor governing catalytic performance is the specific surface area. A higher surface area generally corresponds to more exposed active sites per unit mass, which can enhance both the reaction rate and selectivity toward desired products like acetaldehyde and ethyl acetate. In Cr–Cu–O catalysts, the chromium oxide promotes the dispersion of the copper phase, thereby increasing the surface area.[20-23] In Ce–Cu–O systems, the redox properties of ceria facilitate the activation of copper sites. Consequently, optimizing surface properties is a critical strategy for improving catalytic performance.

This study aims to systematically investigate the role of specific surface area in bioethanol dehydrogenation over Cr–Cu–O and Ce–Cu–O catalysts with varying atomic ratios. The catalysts were synthesized and characterized for their structural, textural, and surface properties. Their activity, product selectivity, and conversion efficiency were evaluated to establish a correlation between surface area and performance. This approach is expected to contribute to both fundamental knowledge in heterogeneous catalysis and the practical development of more efficient catalysts for industrial bioethanol transformation.

## EXPERIMENTAL

### *Catalyst preparation*[25]

Binary chromium-copper oxide catalysts with varying atomic ratios were synthesized by using a co-precipitation method. The synthesis involved mixing aqueous solutions of chromium (III) nitrate and copper (II) nitrate, followed by a multi-stage thermal processing. This included evaporation at 368-373K, drying at 373–393K, thermal decomposition at 523–573 K to stop the evolution of nitrogen oxides, and a final calcination at 823K for 10 hours. The resulting catalysts covered a broad compositional range, with Cr: Cu atomic ratios extending from 9:1 to 1:9.

The Ce–Cr–O catalysts were prepared using a procedure similar to that established for the Cr–Cu–O system. In this approach, aqueous solutions of cerium (III) nitrate and chromium (III) nitrate were coprecipitated under equivalent conditions, then subjected to an identical series of thermal steps involving evaporation, drying, thermal decomposition, and final calcination.

### *Catalytic test*

The catalytic activity of synthesized chromium-copper oxide and cerium-copper oxide catalysts was assessed for bioethanol dehydrogenation. The investigation was carried out in a lab-scale flow reactor. A fixed bed of 5 ml of catalyst (with a particle size of 1.0–2.0 mm) was subjected to a feed of bioethanol at a volume rate of 1200 $h^{-1}$ under a nitrogen carrier gas. The

reaction was studied over a temperature range of 423 to 723K for determining its effect on catalyst performance. Subsequently, the conversion of bioethanol and the yields of the dehydrogenation products were quantified using chromatographic analysis.

The composition and yields of reaction products were determined by gas chromatography using detector and column configurations optimized for different classes of compounds.

Condensable organic products (acetaldehyde, acetone, ethyl acetate) were analyzed using an Agilent 7820A gas chromatograph equipped with a flame ionization detector (FID). Separation was achieved on a 3 m packed column filled with Polysorb-1 sorbent. Nitrogen served as the carrier gas at a constant flow rate of 30 mL·min$^{-1}$. The injector and detector temperatures were maintained at 473 K and 523 K, respectively. The column oven was operated under isothermal conditions, with the temperature selected to ensure efficient separation of oxygenated compounds.

Carbon monoxide (CO) was analyzed using a dedicated gas chromatographic system equipped with a packed column (2 m, activated carbon). Nitrogen was used as the carrier gas at a flow rate of 25 mL·min$^{-1}$. The column temperature was maintained under isothermal conditions optimized for CO separation, while the detector temperature was set at 423 K.

Gaseous products, including butene-1, cis-butene-2, and carbon dioxide, were analyzed using a gas chromatograph equipped with a thermal conductivity detector (TCD). Separation was performed on a packed column under isothermal conditions, with nitrogen as the carrier gas at a flow rate of 30 mL·min$^{-1}$. The TCD temperature was maintained at 473 K to ensure stable detection of permanent gases and light hydrocarbons.

All analyses were conducted under steady-state reaction conditions. Quantification was carried out using external calibration with standard gas and liquid mixtures of known composition. The carbon balance was maintained within ±5%, confirming the reliability and accuracy of the analytical procedure.

*Catalyst characterization*

The textural properties of the catalysts were characterized by low-temperature nitrogen adsorption–desorption measurements conducted at 77 K using a SORBI-MS surface area and porosity analyzer (ZAO META, Russia). Prior to analysis, all samples were degassed under vacuum at 473 K for 3-4 h to remove physically adsorbed moisture and other volatile contaminants. The specific surface area ($S_{BET}$) was determined by applying the multipoint Brunauer–Emmett–Teller (BET) method within the relative pressure ($P/P_0$) range of 0.05–0.30. The total pore volume ($V_p$) was derived from the nitrogen uptake at a relative pressure of approximately 0.99. Pore size distributions and average pore diameters were calculated using the Barrett–Joyner–Halenda (BJH) method applied to the desorption branch of the isotherms.

The crystalline structures of the chromium–copper oxide (Cr–Cu–O) and cerium–copper oxide (Ce–Cu–O) catalysts were investigated by X-ray diffraction (XRD) using a Bruker D2 Phaser diffractometer equipped with Cu Kα radiation (λ = 1.5406 Å) and a nickel filter. Diffraction patterns were collected over a 2θ range of 3–80° with appropriate step size and scan rate to ensure reliable phase identification. The analysis aimed to determine the phase composition and structural characteristics of these binary catalyst systems.

Phase identification was performed by comparison with standard reference patterns from the PDF database. For the Cr–Cu–O catalysts, diffraction peaks corresponding to CuO and $Cr_2O_3$ phases were observed, along with the formation of mixed oxide phases such as $Cu_2CrO_4$, depending on the catalyst composition. In the Ce–Cu–O system, characteristic reflections of fluorite-structured $CeO_2$ and monoclinic CuO were detected. For specific compositions,

particularly those with high copper content, partial reduction of copper species to metallic Cu was also identified.

The average crystallite size ($D$) of the oxide phases was estimated using the Scherrer equation:

$$D = \frac{K\lambda}{\beta cos\theta} \quad (1)$$

Where:

$D$ is the crystallite size (nm),

$K$ is the shape factor (taken as 0.9),

$\lambda$ is the X-ray wavelength (1.5406 Å),

$\beta$ is the full width at half maximum of the selected diffraction peak (in radians),

$\theta$ is the Bragg angle (in radians).

The relative degree of crystallinity ($X_c$) of the catalysts was evaluated by comparing the integrated intensity of the crystalline diffraction peaks with the total scattered intensity, including the amorphous background. The crystallinity percentage was calculated according to:

$$X_c(\%) = \frac{A_{\text{crystalline}}}{A_{\text{total}}} x100 \quad (2)$$

$A_{\text{crystalline}}$ is the cumulative area of all resolved diffraction peaks and $A_{\text{total}}$ represents the total area under the diffraction pattern after baseline correction.

Peak deconvolution and background subtraction were performed to separate overlapping reflections and the amorphous contribution. The crystallinity values of the catalysts were found to vary over a broad range (approximately 40–75%), indicating significant differences in structural order depending on composition.

A pronounced correlation between crystallinity and catalytic performance was observed. Catalysts with higher crystallinity exhibited well-defined oxide phases and enhanced structural stability, whereas samples with lower crystallinity (i.e., higher amorphous content) provided a greater density of defect sites. These defect-rich structures are likely responsible for promoting parallel reaction pathways, including condensation reactions that yield products such as ethyl acetate. Thus, the degree of crystallinity plays a critical role in modulating both activity and selectivity in bioethanol conversion.

## RESULT AND DISCUSSION

The catalytic performance of the Cr–Cu (1:9) catalyst in the bioethanol dehydrogenation reaction is presented in Fig. 1. The onset of the dehydrogenation reaction is observed at 373 K. Upon increasing the temperature to 423 K, acetaldehyde is formed with an initial yield of 23%. Further elevation of the reaction temperature leads to a progressive increase in acetaldehyde yield, reaching a maximum of 34.5%. The productivity of acetaldehyde passes through a maximum at 573K (46.2%). Further temperature increase leads to the formation of carbon dioxide, acetone, ethylene, and ethyl acetate. Fig. 1 shows that bioethanol conversion on the studied catalyst reaches (93.5%) at 723K.

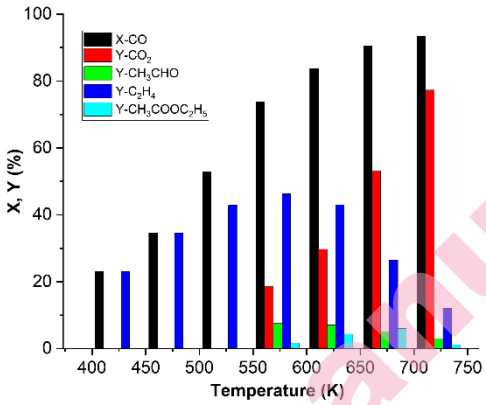


Fig. 1. Investigation of bioethanol dehydrogenation over bimetallic Cr-Cu=1:9 catalyst.

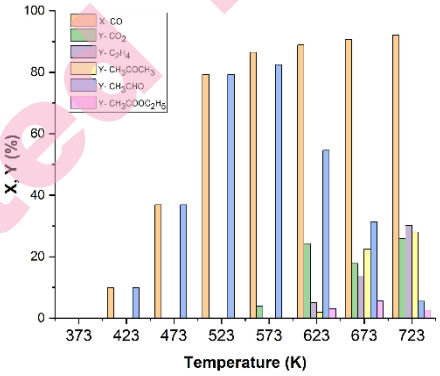


Fig. 2. Investigation of bioethanol dehydrogenation over bimetallic Cr-Cu=6:4 catalyst.

The data in Fig. 2 shows that bioethanol dehydrogenation begins at 423K, producing only acetaldehyde with an initial yield of 9.9%. As temperature increases, other products begin to form. The yield of acetaldehyde itself peaks at 573K, reaching a maximum of 82.5% with a remarkably high selectivity of 97.6%, before declining at higher temperatures due to the formation of competing byproducts.

Product yields are highly dependent on temperature. While ethyl acetate production peaks at 673K, its maximum yield is modest at only 5.6%. The major products are carbon dioxide, ethylene, and acetone, which all reach their highest concentrations at 723K, with significant yields of 25.8%, 30.2%, and 28%,

respectively. This shift towards these byproducts is linked to the catalyst's efficiency, which drives bioethanol conversion to 92.1% at the same temperature.

Research into chromium-copper oxide catalysts demonstrates that temperature critically controls the outcome of bioethanol dehydrogenation. Low temperatures favor the high-yield production of acetaldehyde and its subsequent conversion to ethyl acetate. In contrast, high temperatures (above 573K) trigger different reactions, leading predominantly to a mix of light olefins like ethylene and the complete breakdown of bioethanol into waste products like carbon monoxide and carbon dioxide.

Beyond identifying the reaction pathway, the studies detailed the specific outputs of bioethanol dehydrogenation catalyzed by cerium-copper oxides. The process generates a suite of chemicals, primarily acetaldehyde, acetone, carbon dioxide, ethylene, and ethyl acetate, alongside smaller quantities of other organic fragments from the breakdown of bioethanol. As a key example of this catalytic activity, the performance data for the Ce–Cu catalyst with a 1:9 atomic ratio are explicitly provided in Fig. 3, offering a clear view of its effectiveness in facilitating the reaction.

Over bimetallic cerium-copper oxide catalysts the dehydrogenation of bioethanol products include acetaldehyde, ethyl acetate, acetone, ethylene, and carbon monoxide. Figure 3 illustrates the temperature dependence of the activity of the catalyst Ce-Cu = 1:9 in the dehydrogenation reaction of bioethanol. As can be seen from the Fig. 3, the yields of acetaldehyde, acetone, ethyl acetate and ethylene reach a maximum and then decline with increasing reaction temperature, while the yields of carbon dioxide increase slightly and reach 12.5% at 723K. As the temperature rises, the conversion of bioethanol improves to 78.1% at 573K, after which it stays virtually unchanged.

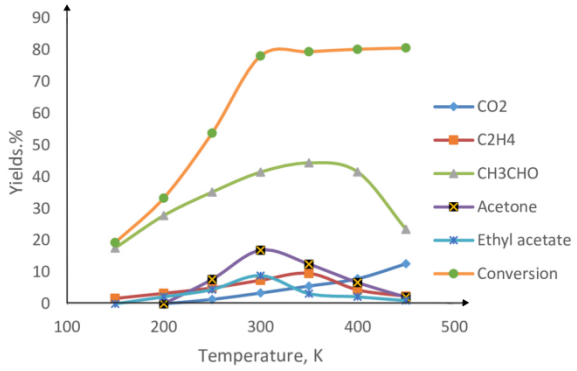


Fig. 3. The influence of temperature on the yield of the products of the dehydrogenation reaction of bioethanol over bimetallic catalyst Ce-Cu =1:9.

The catalytic activity for bioethanol dehydrogenation over the Ce–Cu catalyst with a 1:9 ratio is presented in Fig. 3. The process becomes active at 423K, generating an initial acetaldehyde yield of 15.2%. The yield then climbs progressively with temperature, achieving a maximum conversion of 44.8% at 573K. Following this peak, a decrease in yield is observed, suggesting the onset of secondary reactions or catalyst deactivation at higher temperatures.

The studies demonstrated that the products of bioethanol dehydrogenation over bimetallic cerium–copper oxide catalysts are acetaldehyde, acetone, carbon dioxide, ethylene, ethyl acetate, and a small amount of organic decomposition products of the initial alcohol. As with the reaction at 523K, at 673K the yields of acetone and ethyl acetate also illustrate a bimodal distribution depending on the composition of the cerium–copper oxide catalysts. The results of the bioethanol dehydrogenation reaction at different temperatures over the Ce–Cu = 2:8 catalyst are shown in Table I.

TABLE I. Bioethanol Dehydrogenation over the Ce–Cu = 2:8 Catalyst

| T / K | Yield / % | | | | | Conversion / % |
|---|---|---|---|---|---|---|
| | $CO+CO_2$ | $C_2H_4$ | $CH_3CHO$ | $CH_3COCH_3$ | $CH_3COOC_2H_5$ | |
| 373 | 0 | - | - | 0 | - | 0 |
| 423 | - | - | 6.8 | - | 0 | 6.8 |
| 473 | 0 | - | 12.4 | - | 19.8 | 32.2 |
| 523 | 2.2 | - | 26.6 | 0 | 26.1 | 54.9 |
| 573 | 4.1 | 0 | 34.7 | 10.5 | 23.5 | 72.5 |
| 623 | 5.7 | 7.2 | 27.2 | 18.2 | 17.4 | 75.7 |
| 673 | 7.6 | 14.4 | 18.2 | 23.7 | 12.9 | 76.8 |
| 723 | 41.3 | 2.4 | 9.5 | 14.4 | 10.5 | 78 |

The bioethanol dehydrogenation process is highly sensitive to temperature, as detailed in the table. Beginning at 423K, a 6.8% yield of acetaldehyde is observed. The acetaldehyde yield rises with increasing temperature, achieving a maximum of 34.7% at 573K, but then plummets to 9.5% at 723K. In parallel, ethylene formation follows a similar trend, reaching its own peak yield of 14.4% at 623K. Ethyl acetate generation is activated at 473K and optimizes at 523K with a 26.1% yield. Notably, this peak temperature for ethyl acetate also serves as the starting point for acetone production. Beyond 523K, acetone becomes the dominant product, with its yield escalating to a maximum of 34.7% at 573K. Carbon dioxide formation begins at 523K and increases throughout the studied temperature range, reaching its maximum yield of 41.3% at 723K. According to Table I, bioethanol conversion reaches 78% at 723K over this catalyst.

The data on the activity of the Ce–Cu = 3:7 catalyst in the bioethanol dehydrogenation reaction are given in Table II. The reaction starts at 423K, as in the previous samples, producing 2% ethylene and 1.3% acetaldehyde. With

increasing temperature, acetaldehyde yield reaches a maximum of 33.8% at 573K. Ethylene yield also passes through a maximum, reaching 13.5% at 673K.

TABLE II. Bioethanol Dehydrogenation over the Ce–Cu = 3:7 Catalyst

| T / K | Yield / % | | | | | Conversion / % |
|---|---|---|---|---|---|---|
| | $CO+CO_2$ | $C_2H_4$ | $CH_3CHO$ | $CH_3COCH_3$ | $CH_3COOC_2H_5$ | |
| 273 | 0 | - | - | 0 | - | 0 |
| 423 | 0 | 2 | 1.3 | 0 | 0 | 3.3 |
| 473 | 0 | 3.2 | 9.3 | 1.2 | 7.6 | 21.3 |
| 523 | 1.7 | 4.4 | 23.8 | 6.5 | 19.8 | 56.2 |
| 573 | 6.8 | 6.4 | 33.8 | 16.2 | 13.7 | 76.9 |
| 623 | 13.4 | 10.6 | 23.6 | 31.7 | 5.4 | 84.7 |
| 673 | 18.2 | 13.5 | 14.5 | 42.2 | 1.1 | 89.5 |
| 723 | 24.4 | 4.8 | 9.6 | 47 | 0 | 91.6 |

The thermal decomposition process leads to the formation of oxygenated by-products, including acetone and ethyl acetate, which are first detected at a reaction temperature of 473K. The maximum attainable yields for these key compounds are 47.0% for acetone and 19.8% for ethyl acetate, indicating acetone is the predominant oxygenated product under these conditions. Concurrently, the conversion of bioethanol, the likely feedstock, is also enhanced at higher temperatures. Furthermore, the table indicates that carbon dioxide production follows a continuous upward trajectory across the entire experimental range, culminating in a maximum yield of 24.4% at the highest temperature studied, 723K, suggesting progressive decarbonylation or combustion reactions at more severe conditions.

The results show that bioethanol conversion over this catalyst reaches 91.6% at 723K. Thus, based on the investigation of bioethanol dehydrogenation over binary copper-containing oxide catalysts, the following conclusions can be drawn: up to 573K, bioethanol is mainly converted to ethyl acetate and acetaldehyde over cerium–copper oxide catalysts. At higher temperatures, the main products become acetone and acetaldehyde.

Both catalysts (Fig 4.) exhibit high ethanol conversion, with Ce–Cu–O (75.7%) slightly outperforming Cr–Cu–O (73.8%). However, selectivity patterns differ substantially, reflecting distinct active site chemistries. Cr–Cu–O yields significantly more acetaldehyde (46.2%) than Ce–Cu–O (34.7%), indicating greater selectivity toward direct dehydrogenation. This is attributed to well-dispersed $CuO/Cu^0$ sites and the stabilizing effect of the $CuCr_2O_4$ mixed oxide phase. Ce–Cu–O produces markedly higher yields of ethyl acetate (24.9% vs 1.6%) and acetone (11.2% vs trace), consistent with its bifunctional $CeO_2$ phase and higher density of defect-rich interfacial sites that promote C–C coupling via esterification and ketonization pathways. Cr–Cu–O shows increased formation of

ethylene (7.5% vs 1.5%) and $CO_x$ (18.5% vs 3.4%), suggesting the presence of acidic $Cr_2O_3$ sites and enhanced thermal stability that facilitate dehydration and deep oxidation pathways.

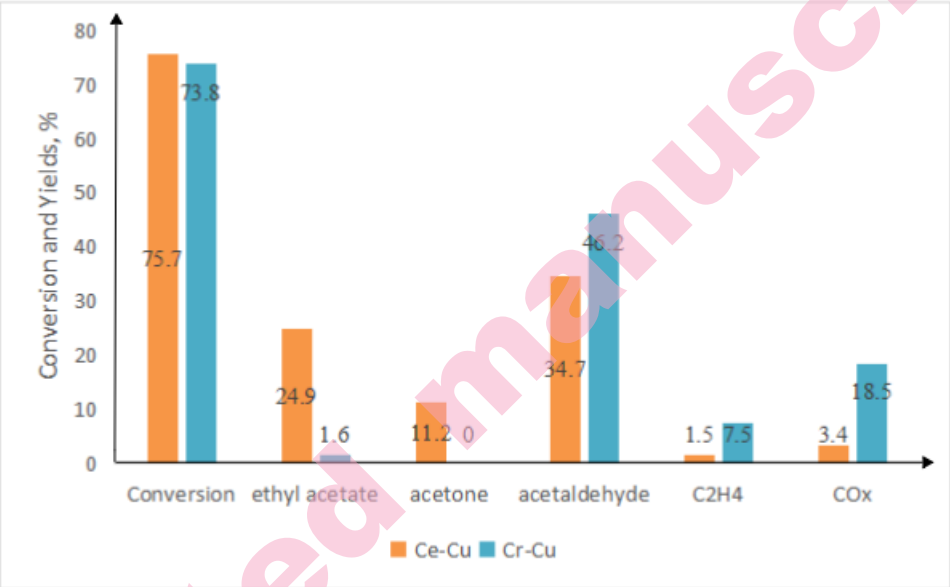


Fig. 4. Effect of Catalyst Composition on product selectivity in bioethanol dehydrogenation (Cr–Cu–O & Ce–Cu–O, 1:9, 573 K)

These results clearly demonstrate that, even under identical reaction conditions, the catalytic behaviour is strongly phase-dependent: Cr–Cu–O favours selective dehydrogenation, whereas Ce–Cu–O promotes a broader reaction network involving condensation and secondary transformations.

The provided Fig. 5 displays the combined X-ray diffraction (XRD) patterns for the nine synthesized samples with varying Chromium-to-Copper (Cr:Cu) atomic ratios. For reference, the standard diffractograms for pure $Cr_2O_3$ and CuO are positioned at the top and bottom, respectively. Analysis of these patterns confirms that all samples within the Cr–Cu–O system consist of a mixture of three distinct phases: chromium oxide ($Cr_2O_3$), copper oxide (CuO), and the composite spinel compound, copper chromite ($CuCr_2O_4$). The systematic variation in the intensity of the characteristic diffraction peaks across the samples provides strong evidence that the proportional relationships between these phases are maintained consistently. X-ray diffraction analysis on all figures showed that all Cr–Cu–O samples contain three phases: $Cr_2O_3$, CuO, and $CuCr_2O_4$.

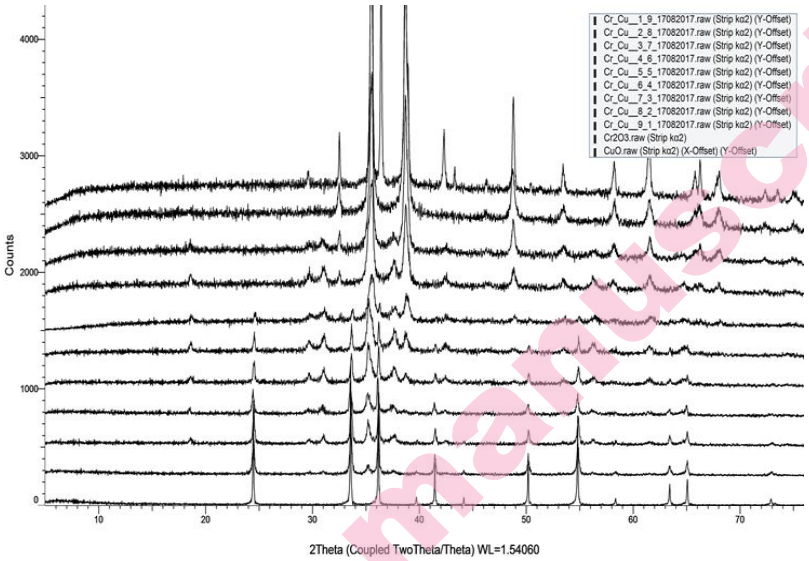


Fig. 5. X-ray diffraction patterns of chromium and copper oxides, and all nine samples of the Cr–Cu–O catalytic system.

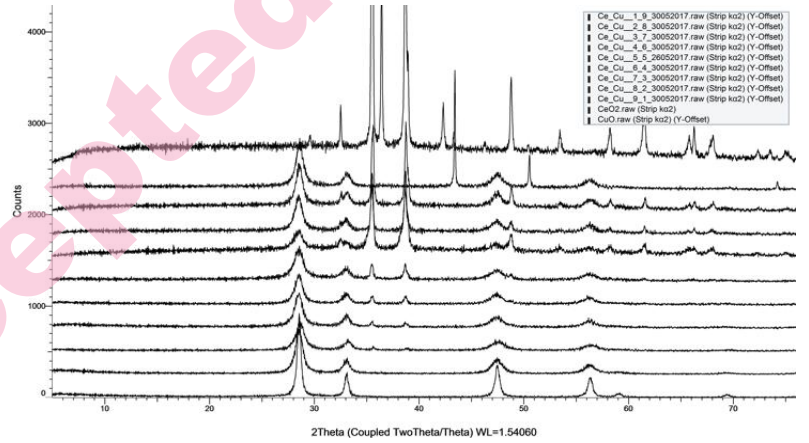


Fig. 6. X-ray diffraction patterns of $CeO_2$ and CuO, and nine Ce–Cu–O catalyst samples.

Fig. 6 shows the diffraction patterns for all nine Ce:Cu ratios. $CeO_2$ and CuO phases were observed in all samples, while metallic Cu appeared in the Ce–Cu = 1:9 composition.

Also Fig. 6 presents the combined diffraction patterns for all Ce:Cu ratios. For comparison, $CeO_2$ and CuO reference diffractograms are included at the start and end. The consistent variation in peak intensities across samples indicates that the phase ratios remain stable. The Ce–Cu–O system forms $CeO_2$, CuO, and, in some compositions, metallic Cu phases (Table III).

TABLE III. Phases Formed in the Ce–Cu–O System

| Ce:Cu Ratio | Formed Phases |
|---|---|
| 1 Ce – 9Cu | $CeO_2$ and Cu |
| 2 Ce – 8Cu | $CeO_2$ and CuO |
| 3Ce – 7Cu | $CeO_2$ and CuO |
| 4 Ce – 6Cu | $CeO_2$ and CuO |
| 5 Ce – 5Cu | $CeO_2$ and CuO |
| 6 Ce – 4Cu | $CeO_2$ and CuO |
| 7 Ce – 3Cu | $CeO_2$ and CuO |
| 8 Ce- 2Cu | $CeO_2$ and CuO |
| 9 Ce – 1Cu | $CeO_2$ and CuO |

Crystallinity in Cr–Cu–O increases from 41.6% to 73.3%. In Ce–Cu–O, it increases slightly from 66.7% to 71.2% with increasing cerium content (Table IV).

In Cr–Cu–O, specific surface area ranges from 9.1 to 14.1 $m^2/g$. Maximum value is observed for Cr–Cu = 8:2. For comparison, $Cr_2O_3$ and CuO have 2.4 and 0.6 $m^2/g$, respectively. The specific surface area of Ce–Cu–O catalysts varies between 5.0 and 17.0 $m^2/g$ (Table V).

TABLE IV. Degree of Crystallinity in the Cr–Cu–O and Ce–Cu–O Systems

| Cr-Cu-O / % | | Ce-Cu-O / % | |
|---|---|---|---|
| Cr:Cu Ratio | Crystallinity / % | Ce:Cu Ratio | Crystallinity / % |
| 1:9 | 41.6 | 1:9 | 66.7 |
| 2:8 | 41.9 | 2:8 | 59.1 |
| 3:7 | 50.2 | 3:7 | 63.0 |
| 4:6 | 57.3 | 4:6 | 52.7 |
| 5:5 | 64.4 | 5:5 | 62.5 |
| 6:4 | 67.1 | 6:4 | 70.4 |
| 7:3 | 69.7 | 7:3 | 67.9 |
| 8:2 | 73.3 | 8:2 | 64.6 |
| 9:1 | 71.2 | 9:1 | 71.2 |

TABLE V. Specific Surface Area of Cr–Cu–O Catalytic System Samples ($m^2/g$)

| Cr/Cu | $Cr_2O_3$ | 1-9 | 2-8 | 3-7 | 4-6 | 5-5 | 6-4 | 7-3 | 8-2 | 9-1 | CuO |
|---|---|---|---|---|---|---|---|---|---|---|---|
| S / $m^2/g$ | 2.4 | 12.5 | 9.1 | 9.9 | 11.4 | 12.5 | 12.5 | 13.7 | 14.1 | 13.3 | 0.6 |
| Ce/Cu | CeO | 1-9 | 2-8 | 3-7 | 4-6 | 5-5 | 6-4 | 7-3 | 8-2 | 9-1 | CuO |
| S / $m^2/g$ | 6.2 | 7.1 | 6.1 | 5.6 | 5.6 | 5.0 | 8.0 | 6.7 | 10.5 | 17.0 | 0.6 |

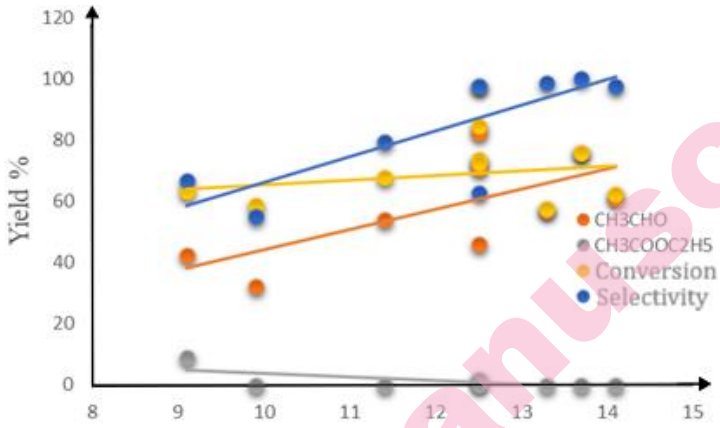


Fig. 7. Effect of specific surface area on the activity of Cr–Cu–O catalysts in bioethanol dehydrogenation (T = 573K). $CH_3CHO$, $CH_3COOC_2H_5$, conversion.

The Fig. 7 illustrates how the specific surface area influences product yields in the bioethanol dehydrogenation reaction over Cr–Cu–O catalysts. As the surface area increases, acetaldehyde yield and bioethanol conversion rise, while ethyl acetate yield decreases. The selectivity toward acetaldehyde also improves with increasing surface area.

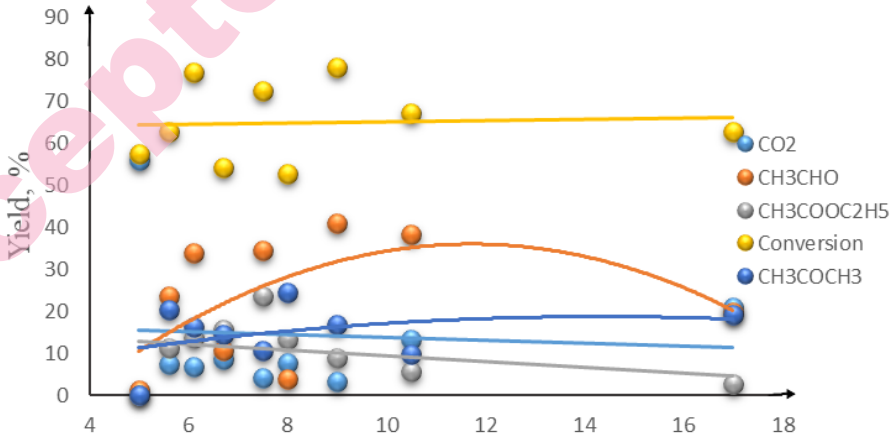


Fig. 8. Effect of specific surface area on the activity of Ce–Cu–O catalysts in bioethanol dehydrogenation (T = 300°C).

The Figure 8 illustrates how the specific surface area of Ce–Cu–O catalysts governs the resulting product yields. A non-monotonic relationship is observed for acetaldehyde and acetone, whose yields pass through a distinct maximum. In contrast, the formation of ethyl acetate and the complete oxidation product $CO_2$

are disfavored on catalysts with higher surface areas. Increasing surface area in Cr–Cu–O catalysts leads to higher acetaldehyde yield and bioethanol conversion. In Ce–Cu–O catalysts, acetaldehyde and acetone yields pass through maxima with increasing surface area, while ethyl acetate and $CO_2$ yields decrease. Bioethanol conversion is only slightly affected by surface area in Ce–Cu–O.

To rationalize the influence of specific surface area on product distribution, it is essential to distinguish between total surface area and catalytically active sites. In the Cr–Cu–O and Ce–Cu–O systems, the surface is not uniformly active; rather, catalytic performance is governed by specific active centers associated with particular phases and interfacial structures. XRD analysis (Figs. 5–6) confirms that the catalysts are multiphase systems. In the Cr–Cu–O system, CuO, $Cr_2O_3$, and $CuCr_2O_4$ are present; in the Ce–Cu–O system, $CeO_2$ and CuO are observed, with metallic Cu appearing in selected compositions. Each phase contributes distinctively to catalytic behaviour:

- CuO and $Cu^0$ serve as primary sites for ethanol dehydrogenation, favouring acetaldehyde formation;
- Mixed oxide phases (e.g., $CuCr_2O_4$) and phase boundaries facilitate C–C coupling and condensation reactions, promoting ethyl acetate formation;
- $CeO_2$ acts as a promoter, enhancing oxygen mobility and stabilizing dispersed copper species, thereby modulating both activity and selectivity.

Thus, the dependence of product yields on specific surface area (Figs. 7–8) cannot be interpreted solely in terms of total available surface. Instead, surface area reflects the dispersion, accessibility, and relative abundance of distinct active sites.

Importantly, surface area and crystallinity are interrelated. Catalysts with lower crystallinity (higher amorphous content) exhibit a greater density of structural defects and interfacial sites, which promote secondary reactions such as esterification and condensation, leading to increased ethyl acetate yields. Conversely, highly crystalline catalysts possess well-defined oxide phases with fewer defect sites, favouring selective dehydrogenation to acetaldehyde.

Although direct quantification of individual phase activity is challenging in such multicomponent systems, correlative analysis combining compositional variation, XRD phase identification, crystallinity (Table IV), and catalytic data (Tables I–II, Figs. 7–8) provides strong evidence that:

- Acetaldehyde formation is primarily associated with Cu-based active sites;
- Ethyl acetate formation is linked to defect-rich and interfacial sites;
- Total conversion depends on the combined contribution of all accessible active centres.

Consequently, the influence of specific surface area on catalytic performance is phase-dependent and site-specific, explaining why different reaction products respond differently to changes in surface properties.

## CONCLUSION

A comparative investigation was conducted into the catalytic dehydrogenation of bioethanol using two distinct binary oxide systems: chromium-copper (Cr–Cu–O) and cerium-copper (Ce–Cu–O). The study revealed a significant divergence in product selectivity between the two catalysts. The Cr–Cu–O system primarily facilitated the formation of acetaldehyde as the major dehydrogenation product, alongside valuable oxygenates such as acetone and ethyl acetate, as well as the dehydration product ethylene and fully oxidized carbon dioxide. In contrast, the Ce–Cu–O catalysts produced a similar suite of compounds—including acetaldehyde, acetone, ethyl acetate, and ethylene—but also demonstrated a propensity for further decomposition, evidenced by the generation of carbon monoxide in addition to carbon dioxide.

It was shown that binary chromium–copper oxide catalysts consist not only of chromium and copper oxide phases but also of the $Cu_2CrO_4$ compound phase, with crystallinity varying between 41.9% and 73.8%. In bioethanol dehydrogenation over these catalysts, an increase in crystallinity leads to the yield of acetaldehyde and the selectivity of bioethanol dehydrogenation to acetaldehyde passing through a minimum. The study of binary cerium–copper oxide systems showed that, except for the Ce:Cu = 1:9 ratio, $CeO_2$ and CuO phases are formed in all compositions. At Ce:Cu = 1:9, however, $CeO_2$ and elemental Cu phases are observed, and their crystallinity increases from 52.7% to 71.2%. It was determined that in bioethanol dehydrogenation over cerium–copper oxide catalysts, acetaldehyde formation is predominant in samples with medium crystallinity, whereas ethyl acetate is mainly produced in poorly crystalline samples. The specific surface area of binary chromium–copper oxide catalysts varies between 9.1–14.1 $m^2/g$, while for cerium–copper oxide catalysts it varies between 5.0–17.0 $m^2/g$, depending on the composition. It was established that changes in the specific surface area influence the yields of reaction products differently.

When bioethanol is dehydrogenated using chromium-copper oxide catalysts, it produces a range of products including acetaldehyde, ethyl acetate, acetone, ethylene, carbon monoxide, and carbon dioxide. These catalysts are composed of a mixture of separate chromium and copper oxide phases, along with a distinct compound known as copper chromite ($CuCr_2O_4$).

Their degree of crystallinity ranges from 42.6% to 73.8%. In bioethanol dehydrogenation over binary (Cr-Cu oxide) catalysts, increasing crystallinity enhances acetaldehyde yield, bioethanol conversion, and the selectivity of the reaction toward acetaldehyde. The effect of specific surface area on the activity of the binary chromium–copper oxide catalytic system was also studied. It was established that an increase in surface area increases acetaldehyde yield and bioethanol conversion to acetaldehyde. For the Cr–Cu = 6:4 catalyst, the highest acetaldehyde yield was 82.5%, with a selectivity of 97.6%.

## SUPPLEMENTARY MATERIAL

Additional data are available electronically at the pages of journal website: https://www.shd-pub.org.rs/index.php/JSCS/article/view/13693, or from the corresponding author on request.

## И З В О Д

### УТИЦАЈ САСТАВА И ПОВРШИНСКИХ СВОЈСТАВА КАТАЛИЗАТОРА НА СЕЛЕКТИВНУ КАТАЛИТИЧКУ ДЕХИДРОГЕНИЗАЦИЈУ БИОЕТАНОЛА

GUNEL R. AZIMOVA[1*], SELIME MAMMADOVA[2], TURANA A. BABAYEVA[3], KONUL SH. ALAKBAROVA[1], VILAYET S. MAMMADOV[1], TIANJIN LI[4], ELMIR M. BABAYEV[1,3**]

*[1]Chemistry Institute, H.Javid Ave. 113, AZ1143, Baku, Azerbaijan, [2]Azerbaijan State Oil and Industry University, Azadlıq 20, AZ 1010, Baku, Azerbaijan, [3]Baku Engineering University, Hasan Aliyev st., 120, AZ0101, Khirdalan, Azerbaijan, and [4]Energy Research Institute, Qilu University of Technology, Shandong Academy of Sciences, Jinan 250014, PR China.*

У овом раду представљена је упоредна анализа дехидрогенизације етанола коришћењем Cr-Cu-O и Ce-Cu-O катализаторских система. У случају Cr-Cu-O катализатора, биоетанол се преводи у низ производа укључујући ацеталдехид, ацетон и етилен. Напредна карактеризација је показала да су испитивани катализатори структурно сложени, јер садрже не само појединачне оксиде бакра и хрома, већ и једињење, $Cu_2CrO_4$. Кључни резултат је јасна веза између структуре и својстава: кристалиничност катализатора, која се кретала у широком распону од 41,9% (углавном аморфни) до 73,8% (високо кристалинични), има велики утицај на његову каталитичку активност. Ce-Cu-O систем је преводио биоетанол у разноврсну смешу производа као што су ацеталдехид, ацетон и етил-ацетат, што указује на истовремено одвијање више реакција, укључујући дехидрогенизцију и кондензацију. Различити састави најчешће резултирају одвојеним фазама $CeO_2$ и CuO, осим при односу Ce:Cu од 1:9. При овом односу, материјал се редукује тако да поред $CeO_2$ настаје и елементарни бакар, а не CuO, а његова кристалиничност се повећава са 52,7% на 71,2%.

(Примљено 27. децембра 2025; ревидирано 21. јануара 2026; прихваћено 11. маја 2026.)

## REFERENCES

1. M. A. K. Joyia, M. Ahmad, Y. F. Chen, M. Mustaqeem, A. Ali, A. Abbas, M. A. Gondal, *Energy Convers. Manag.* **321** (2024) 119037 (https://doi.org/10.1016/j.enconman.2024.119037)
2. S. Jain, S. Kumar, *Energy* **296** (2024), 131130 (https://doi.org/10.1016/j.energy.2024.131130)
3. A. S. Dibazar, A. Aliasghar, A. Behzadnezhad, A. Shakiba, M. Pazoki, *Biomass Convers. Biorefin.* **14** (2024) 20679 (https://doi.org/10.1007/s13399-023-04288-5)
4. K. Mihajlovski, M. Milić, D. Pecarski, S. Dimitrijević-Branković, *J. Serb. Chem. Soc.* **86** (2021) 651 (https://doi.org/10.2298/JSC210308032M)
5. M. H. Morad, *Arab. J. Chem.* **17** (2024) 105560 (https://doi.org/10.1016/j.arabjc.2023.105560)
6. E. S. Mamedov, B. A. Babaeva, S. E. Mamedov, N. F. Akhmedova, F. S. Kerimli, *Mosc. Univ. Chem. Bull.* **77** (2022) 222 (https://doi.org/10.3103/S002713142204006X)

7. I. M. S. Anekwe, B. Oboirien, Y. M. Isa, *Biofpr.* **18** (2024) 686 (https://doi.org/10.1002/bbb.2536)
8. B. Thangaraj, W. Monama, E. Mohiuddin, M. M. Mdleleni, *Bioresour. Technol.* **409** (2024) 131230 (https://doi.org/10.1016/j.biortech.2024.131230)
9. R. Lei, Z. Chen, Q. Xu, N. Wang, Y. Qin, T. Wang, X. Lin, X. Qiu, *Green Chem.* **27** (2025) 9643 (https://doi.org/10.1039/D5GC02486B)
10. G. Busca, E. Spennati, P. Riani, T. K. Phung, G. Garbarino, *J. Environ. Chem. Eng.* **13** (2025) 119648 (https://doi.org/10.1016/j.jece.2025.119648)
11. S. Liu, Y. Meng, C. Luo, H. Zhu, Y. Song, H. Zhang, T. Wu, *Int. J. Hydrogen Energy.* **86** (2024) 1414 (https://doi.org/10.1016/j.ijhydene.2024.08.413)
12. P. G. Choi, T. Ohno, T. Masui, N. Imanaka, *J. Environ. Sci.* **36** (2015) 63 (https://doi.org/10.1016/j.jes.2015.04.017)
13. D. Yu, W. Dai, G. Wu, N. Guan, L. Li, *Chin. J. Catal.* **40** (2019) 1375 (https://doi.org/10.1016/S1872-2067(19)63378-4)
14. C. Autthanit, W. Chatkaew, P. Praserthdam, B. Jongsomjit, *J. Environ. Chem. Eng.* **8** (2020) 103547 (https://doi.org/10.1016/j.jece.2019.103547)
15. W. Tian, B. Jongsomjit, D. Pjontek, J. E. Herrera, *Mol Catal.* **483** (2020) 110717 (https://doi.org/10.1016/j.mcat.2019.110717)
16. A. Singh, G. P. Rangaiah, *Ind. Eng. Chem. Res.* **56** (2017) 5147 (https://doi.org/10.1021/acs.iecr.7b00273)
17. F. Fang, Y. Guo, *Chin. J. Catal.* **39** (2018) 566 (https://doi.org/10.1016/s1872-2067(17)62996-6)
18. P. H. Finger, T. A. Osmari, M. S. Costa, J. M. C. Bueno, J. M. R. Gallo, *Appl. Catal. A-Gen.* **589** (2020) 117236 (https://doi.org/10.1016/j.apcata.2019.117236)
19. S. H. Mammadova, K. X. Aghayeva, *Chem. Prob.* **18** (2020) 199 (https://chemprob.org/wp-content/uploads/2025/10/199-206.pdf)
20. A. Makoye, A. Vikar, A. B. Nacsa, R. Barthos, J. Valyon, F. Lónyi, T. Nagy, *Catalysts* **15** (2025) 709 (https://doi.org/10.3390/catal15080709)
21. M. Ngcobo, P. R. Makgwane, M. K. Mathe, *Appl. Catal. O: Open.* **193** *(*2024)193 206976 (https://doi.org/10.1016/j.apcato.2024.206976)
22. S. Said, M. Riad, *J. Phys. Chem. Sol.* **205** (2025) 112789 (https://doi.org/10.1016/j.jpcs.2025.112789)
23. C. Tian, Y. Yue, C. Miao, W. Hua, Z. Gao, *Catalysts* **14** (2024) 541 (https://doi.org/10.3390/catal14080541)
24. Y. Zhang, Y. Wang, X. Guan, H. Li, X. Nie, Y. Liang, X. Bao, X. Li, F. Wang, *J. Catal.* **426** (2023) 86 (https://doi.org/10.1016/j.jcat.2023.06.030)
25. Y. A. Fionov, S. G. Chuklina, K. S. Khlusova, A. V. Fionov, A. I. Zhukova, *Magn. Reson. Chem.* **61** (2023) 427 (https://doi.org/10.1002/mrc.5353)
26. C. K. F. Monguen, S. Daniel, Z. Y. Tian, *Chem. Eng. J.* **474** (2023) 145769 (https://doi.org/10.1016/j.cej.2023.145769)
27. S. Preedavijitkul, C. Autthanit, S. Jadsadajerm, C. Sricharoen, P. Praserthdam, B. Jongsomjit, *J. Taiwan Inst. Chem. Eng.* **147** (2023) 104895 (https://doi.org/10.1016/j.jtice.2023.104895).